Photoluminescence characterization of defects in Si and SiGe structures

2000 J. Phys.: Condens. Matter 12 10105

(http://iopscience.iop.org/0953-8984/12/49/310)

J. Phys.: Condens. Matter **12** (2000) 10105–10121. Printed in the UK PII: S0953-8984(00)17838-5

Photoluminescence characterization of defects in Si and SiGe structures

V Higgs†, F Chin†, X Wang†, J Mosalski† and R Beanland‡

† Bio-Rad Micromeasurements, Hemel Hempstead HP2 7TD, UK
‡ Marconi Caswell Ltd, Towcester, Northamptonshire NN12 8EQ, UK

Received 9 October 2000

Abstract. Low-temperature photoluminescence (PL) spectroscopy is a very sensitive tool to investigate the presence of dislocations in Si. The main dislocation-related bands (D1–D4) have been attributed to a wide range of causes, either intrinsic properties of the dislocation or impurity related. PL is a competitive recombination process and the non-radiative processes need to be measured to understand the overall effect of impurities. PL spectroscopy samples a large volume in comparison to the dislocation itself and therefore gives an average effect. High-resolution room-temperature PL mapping (SiPHER) has been used to detect defects in both Si and SiGe wafers. Whole-wafer PL maps reveal the presence of slip on 300 mm Si wafers. Comparison studies with defect etching show that there is a one-to-one correlation between defects detected in the PL micro-scans and those revealed by defect etching. Whole-wafer mapping has revealed a number of different defect types in SiGe epilayers. The ability to record whole-wafer PL maps facilitates the rapid identification of inhomogeneities and defects. High-resolution PL micro-maps showed the defect area to contain a high density of misfit dislocations, and the nucleation site has strong non-radiative recombination. One common defect type was analysed using plan view transmission electron microscopy (TEM) and optical microscopy; these results revealed the presence of a high density of defect loops and stacking faults consistent with the high recombination rate at the defect site.

1. Introduction

The optical and electrical activity of defects in semiconductors has been studied in detail by numerous methods. Low-temperature photoluminescence (PL) spectroscopy on dislocations in Si has long established that certain luminescence features can be attributed to the presence of dislocations. The main dislocation features are the D1–D4 bands (D bands) [1]. The D1 and D2 bands have been attributed to the intrinsic properties of dislocations, such as electronic transitions at the stacking fault between the dislocations, transitions at kinks and reconstructed sites at the dislocation core and even to point defects trapped in the dislocation strain field [2], whereas D3 and D4 are considered to be associated with electronic transitions at the dislocation core [2]. In these earlier studies there was no clear evidence that transition metal impurities may have played a role in the dislocation origin. The detection of PL bands due to the radiative transitions at dislocations is in direct competition with non-radiative processes. Clearly these processes need to be monitored to obtain a clear interpretation of the D-band intensity variation. Also PL spectroscopy samples a large sample volume (typically hundreds of μm^3 depending on the exciton diffusion length) compared to the dislocation density, therefore the spectrum samples both the locations where the dislocations are present and dislocation free regions.

0953-8984/00/4910105+17$30.00

Therefore for low dislocation densities the PL spectrum is averaged over regions where there are no dislocations present.

More recently there is clear evidence that the transition metal impurities may play a key role in the dislocation-related luminescence [3]. Combined cathodoluminescence (CL) and electron-beam-induced current (EBIC) studies have produced a clearer picture of the role of impurities on the activity of dislocations in Si and SiGe [4]. In light of the renewed interest in understanding the optical and electrical activity of dislocations, the PL results will be reviewed and summarized.

From a technological point of view it is increasingly important to detect the presence of dislocations irrespective of their electrical activity in Si, because subsequent device processing of Si wafers containing dislocations will almost certainly lead to poor device performance and low reliability. A new room-temperature PL method (called SiPHER) has been developed to detect defects in the near-surface region of Si wafers and SiGe structures [5]. Wafer maps (up to 300 mm) can be readily acquired and areas of interest can be scanned at high resolution ($\approx$1 μm). The excitation laser beam is modulated to confine the photogenerated carriers; defects are detected due to the reduction of the localized recombination lifetime. Examples will be shown of PL maps revealing dislocations in Si, and misfit dislocations in SiGe.

2. Review of low temperature PL studies on defects

Drozdov *et al* [1] showed that four lines were associated with dislocations produced in plastically deformed Si. They labelled the four lines D1 (0.812 eV), D2 (0.875 eV), D3 (0.934 eV) and D4 (1.00 eV). The PL intensity of these bands scaled with dislocation density. Suezawa and co-workers [6] have carried out a more extended study: they investigated the effect of impurities, deformation temperature and dislocation morphology. They concluded that impurities do not have a marked effect on the recombination processes and D1 and D2 are probably related to kinks on the dislocation. Similarly, Weronek *et al* [7] stated that the D-band recombination is independent of impurities trapped at the dislocations and they attributed D1 and D2 to the stacking fault between two Shockley partial dislocations. They also demonstrated that the D-band intensity was reduced following deliberate metal contamination in the case of Fe and Cu. A more detailed investigation was carried out by Sauer *et al* [2], where they studied dislocations deformed in a well defined manner. PL from uniaxial stress measurements indicated that D1 and D2 originated at tetragonal defects with random orientation. These bands may be connected with deformation-induced point defects in the dislocation strain field.

An alternative model was proposed based on a recombination of a 1D exciton bound within the dislocation strain field [8]. It was suggested that the classification of the D bands could be attributed to the dislocation Burgers vector. D2 was assigned to recombination at a Lomer–Cottrell dislocation and D1 its phonon replica. Also D4 was attributed to the dislocation exciton at the dissociated dislocation. D3 was assigned to its phonon replica. Kittler *et al* suggested that the recombination model due to Kveder originally developed to explain temperature dependent EBIC contrast behaviour for dislocations could be utilized to explain the radiative recombination at defects [9]. This model couples recombination at shallow levels with the extrinsic deep levels surrounding them.

Suezawa *et al* [10] have shown that dislocations in CZ Si ([O] 8×10^{17} cm^{-3}) show D1 and exhibit a PL reduction compared to dislocated FZ Si, whereas Osipyan *et al* [11] observed a considerable increase in the D1 intensity upon annealing CZ Si ([O] $> 10^{17}$ cm^{-3}). A more recent investigation by Pizzini *et al* [12] has shown that dislocations produced in CZ Si at low temperature ($T = 650\,^{\circ}$C) produce D bands.

The D-band features are sensitive to excitation wavelength. It was shown that the D1 and D2 features are more dominant in the PL spectrum when using above-band-gap excitation [2], whereas for below-band-gap measurements (Nd-YAG laser) the D1 and D2 states are significantly reduced. Suezawa and Sumino had also observed a similar effect when using an Ar laser or 1 μm light from a halogen lamp [10].

A PL study of dislocations in $Si_{1-x}Ge_x$ alloys with different compositions revealed some intriguing effects [13]. The D1 and D2 peak positions did not depend on alloy composition, while D3 and D4 showed a shift in energy from Si to Ge. From the observed behaviour it was proposed that D1 and D3 were the phonon replicas of D2 and D4. The D2 band is independent of alloy composition and may be connected with an internal transition between two deep states. D4 was likely to be connected with excitonic recombination at dislocations.

2.1. Influence of transition metal contamination

To explore the influence of transition metal contamination Higgs *et al* [3] produced plastically deformed Si containing dislocations (10^4–10^8 cm^{-2}) in a quartz stress cell. Also they pre-selected Si samples that were believed to be free of transition metal impurities ($<10^{11}$ cm^{-3}). The as-deformed samples contained no D-band luminescence and no detectable EBIC contrast. Only following deliberate contamination with Cu, Fe or Ni were the dislocation-related bands observed and the dislocations became visible in EBIC micrographs. D-band position was independent of the different metal contamination treatments.

Further studies characterizing epitaxial stacking faults and oxidation-induced stacking faults showed that the level of contamination had a critical effect on the D1 and D2 intensity [14]. Following deliberate surface contamination and annealing, the D-band features were observed; a maximum intensity was observed for a contamination level of $\approx 4 \times 10^{12}$ atoms cm^{-2}. Following further contamination D1 and D2 reduced in intensity. Analysis using transmission electron microscopy (TEM) revealed no precipitates at low contamination levels but at high contamination levels (when the D1 and D2 bands were quenched) metal precipitates were observed on the bound partial dislocations. It was suggested that, as the level of contamination increased, precipitates were formed which absorbed the centres responsible for dislocation-related recombination.

The effect of transition metal contamination has also been investigated for dislocations in SiGe/Si epilayers [15]. Following low levels of intentional Cu contamination and annealing at 700 °C, all the D bands can be observed. CL imaging revealed that the D3 and D4 bands were dominant at the misfit dislocations whereas D1 and D2 bands increased in signal intensity at the dislocation and were also present in between the dislocations. Similar results were found for Fe and Ni. However, for samples that received much higher (Ni, Fe or Au) contamination levels CL images showed that the D1 and D2 features were observed only in between the dislocations. TEM analysis identified small ($\approx$500 nm) isolated $NiSi_2$ precipitates along the misfit dislocations in the Ni-contaminated sample. The Au-contaminated sample contained small metal-related precipitates ($\approx$50 nm). The CL results were explained in terms of the competition between the centres responsible for radiative recombination and non-radiative transitions. Following low levels of contamination sufficient metal is available that the D bands can be observed. After much greater contamination metal-related precipitates are formed along the dislocations and these metal-related precipitates introduce mid-gap states. These deep levels are much more efficient recombination centres and now non-radiative recombination is more dominant quenching the radiative recombination.

The deliberate metal contamination experiments of Weronek *et al* [7] can easily be explained on the basis of enhanced non-radiative recombination, because they introduced

sufficient contamination (Cu or Fe) to produce metal precipitates and then observed a significant reduction in the D-band intensity.

2.2. Dislocations in CZ Si

There have been a number of previous results already reporting a conflicting view regarding the effect of oxygen on the D bands. A very careful study on dislocations in deformed CZ and FZ Si produced some intriguing results. Higgs [16] showed that PL spectra recorded from CZ Si samples ([O] $= 10^{17}$–10^{19} cm^{-3}) deformed at 700 °C for 15 minutes contained the D-band features. As the deformation time increased (>2 hours) the D-band features were not observed. This effect was more rapid for samples containing more oxygen. IR spectra showed that there were no changes in the bulk oxygen levels for deformation treatments at 700 °C. Control deformation experiments using FZ Si gave no contamination during deformation. It was suggested that the presence of the D bands in the as-deformed material may be caused by the presence of residual metal impurities in the CZ starting material. However, following deformation at a higher temperature ($T = 800$ °C, 15 minutes) no D bands were observed, which is suggested to be due to oxygen segregation producing efficient non-radiative recombination at the dislocations. As the deformation time increased D1 and D2 features were observed, which corresponded to a marked loss of interstitial oxygen (5–10%). It was proposed that the presence of the D1 and D2 bands is related to oxygen segregation producing Si interstitials, which can interact with residual metal contamination.

2.3. Depth dependence of PL bands

As already discussed there have been some clear effects of the excitation wavelength on the intensity of the D bands [2, 10]. The depth dependence of the D1 and D2 features was investigated using chemical etching to remove material and then a PL spectrum was recorded [16]. The PL spectra were recorded using 459.7 nm excitation to give maximum depth discrimination. The D1 and D2 features decreased in intensity nearly tenfold after removing only 1500 nm. These results clearly showed that the centres responsible have point-defect-like properties. These centres are formed at the surface because the Si surface can act as a sink for metals and intrinsic point defects. These results are also supported by the previous studies [2, 10] showing that the centres responsible for D1 and D2 are preferentially formed at the Si surface. It has also been shown that the D1 and D2 bands can be enhanced by rapid thermal quenching of the sample supporting the proposal that point defects are involved [14].

2.4. Spatial distribution of D bands

PL measurements sample a very large volume compared to the size of the dislocation structures. Spatial measurements are required to ascertain the spatial location of the D-band features. CL imaging was used to characterize dislocations in Si and SiGe epilayers [17]. The PL spectrum from a plastically deformed Si sample contained the characteristic D1–D4 bands. The CL images show that the D3 and D4 lines were located along the slip planes. This was clarified by recording CL spectra and placing the electron beam at different locations. The CL spectrum on the slip line contained D3 and D4 only whereas the D1 and D2 bands in the spectrum were observed between the slip planes. Low-temperature PL mapping experiments were recorded from dislocations produced in CZ Si [18]. These experiments also showed the same spatial distribution of the D bands, D1 and D2 at the locations in between the dislocations and D3 and D4 at or near the dislocation position.

2.5. D1 and D2 can be produced without extended defects?

The CL imaging experiments and depth dependences seem to suggest that D1 and D2 have point defect characteristics. This raises the question of whether these recombination centres can be created without extended defects. This was investigated by Higgs [16] using deliberate contamination combined with low-temperature oxidation. After oxidation of a n-type FZ Si sample PL spectra contained only the band edge features. Following Cu contamination ($\approx 4 \times 10^{10}$ atoms cm^{-2}) prior to oxidation ($T = 700\,^{\circ}$C) the PL spectrum contained D1 and D2 features. Similar results were observed for p-type Si but the D-band intensity was much lower. However, following intentional Cu contamination and annealing only the characteristic Cu spectrum is observed. To explain these results it was suggested that both metal contamination and Si interstitials are required to generate the D1 and D2 features. Si interstitials are produced during the oxidation process and the transition metal contamination may facilitate the nucleation of Si interstitial clusters. Such complexes are known to form with C, B or Al in Si [16].

2.6. SiGe epilayers

The influence of Cu contamination on the recombination properties of misfit dislocations has been studied using variable-temperature EBIC measurements [19]. It was found that the EBIC contrast temperature behaviour ($c(T)$) could be used to characterize the contamination level of the dislocations. The results are schematically illustrated in figure 1. In the as-grown material the dislocations (denoted type II) were found to show a weak contrast at low temperature ($T = 80$ K). Following low Cu contamination (Cu = 1 ppb in solution) and then annealing, the low-temperature contrast showed a marked increase but the dislocations could still not be observed at room temperature (denoted type 2). After increasing the contamination level further (Cu = 15 ppb) the dislocations exhibit contrast throughout the whole temperature range ($T = 80$–300 K) (denoted type 1). A much higher contamination treatment (Cu = 1 ppm) produced a dramatic increase in the EBIC contrast (denoted type I). TEM revealed that these samples now contained Cu silicide precipitates connected with the misfit dislocations. The type I behaviour of dislocations was interpreted as due to Cu silicide acting as Schottky barriers enhancing recombination. Type 1 and type 2 contrast variation could be explained using Schottky–Read–Hall recombination statistics. Dislocation type 1 behaviour was controlled by mid-gap levels, while shallow dislocation levels were responsible for type 2 behaviour. Finally it was suggested the type II behaviour observed in the as-grown material could be associated with the true intrinsic dislocation. Hydrogen plasma treatment was found to transform the type 1 behaviour into the type 2, but it could not restore the original type II behaviour. Type I was unaffected by the hydrogen treatment.

It was also found that no dislocation-related PL bands were detected for the samples containing dislocations with type II and type I character (denoted in figure 1), whereas the D bands were observed in the samples containing dislocations with either type 1 or type 2 behaviour. Clearly the absence of the D bands does not have a unique interpretation, because D bands are not observed for dislocations produced under 'clean' conditions or after high metal contamination. Comparative studies are necessary to investigate both non-radiative and radiative processes to understand the overall influence of metal contamination.

The results in this section have shown that impurities play a key role in the origin of the dislocation-related luminescence and that low-temperature PL spectroscopy is a very sensitive technique to investigate the complex chemistry of defects and impurities. However PL samples a relatively large volume compared to the defect itself and the detection of the defects using PL

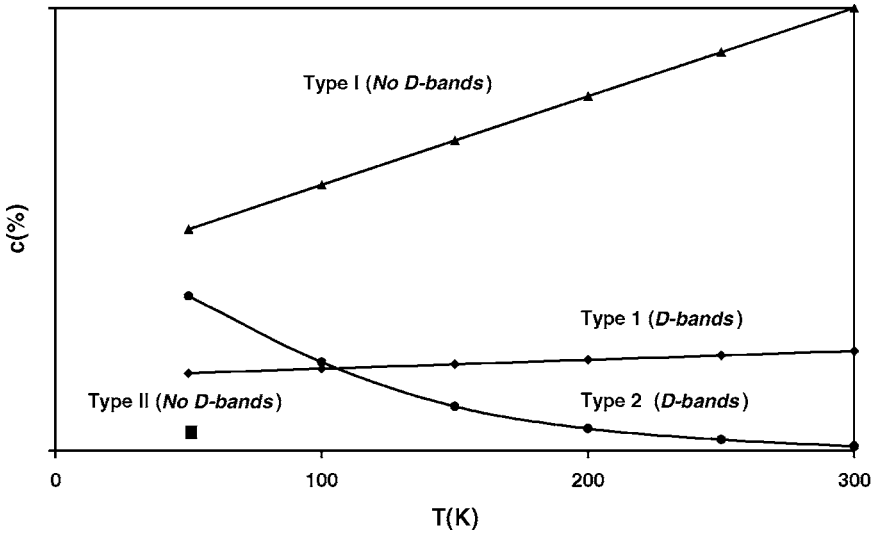

Figure 1. Temperature-dependent EBIC contrast c (%) results for misfit dislocations after Cu contamination.

is complicated because recombination is a competitive process. Therefore the absence of the D bands could suggest that there are no defects present or that impurities around the defects have quenched the radiative recombination. It has been shown that PL/CL mapping can be used to identify the presence of defects using the D-band intensity. Quite clearly defects are more reliably detected using the intensity of band edge radiative recombination intensity [4]. It has already been confirmed that the band edge PL at room temperature is directly correlated with the minority carrier lifetime [20]. This process is very sensitive to the presence of non-radiative recombination at the defect. The application of room-temperature PL mapping using this principle for assessing the quality of Si and SiGe epilayers is demonstrated in the next section.

3. Experiment

Room-temperature PL measurements were obtained using SiPHER [5]; whole wafers (150–300 mm diameter) and small sample sections were measured. For near-surface characterization the wafer or sample was excited using a 532 nm frequency doubled laser. An *in situ* laser marking capability was also used, so that areas of interest could be marked for cross correlation studies. A second image was also recorded simultaneously, which is a reflected laser microscopic image of the sample surface (the 'surface map image'). These two images are point to point exact so that any surface-related structure could be identified and excluded from the analysis.

Samples were also examined by optical microscopy using differential interference contrast (DIC). Regions of interest were identified and subsequently examined by scanning probe microscopy and plan view TEM. Scanning probe microscopy was performed on a Digital Instruments D5000 operating in non-contact mode. Plan view TEM specimens were prepared by mechanical back thinning and jet etching to electron transparency using a 5:1 nitric:HF etchant.

For combined defect etching and defect detection using PL mapping, Si wafers (p-type 10 Ω cm) were thermally processed by a Si wafer supplier to generate a range of different

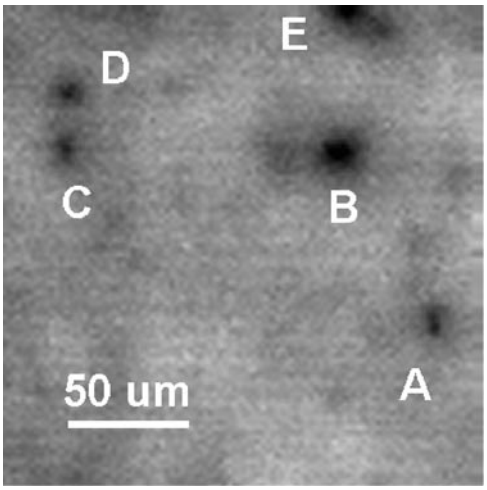

Figure 2. PL map revealing individual defects prior to defect etching.

defects. The wafers were first laser marked and then these regions were scanned to obtained the defect density. The wafers were returned for defect etching and independent defect counting.

A number of 300 mm Si wafers, which underwent thermal treatment, were measured to investigate the presence of slip. Also a number of 300 mm epilayers were also analysed on the wafer back surface to detect the presence of slip.

A selection of SiGe epilayers with different thickness and composition from different suppliers was characterized using SiPHER. Because of the commercial nature of these results, the wafers are denoted as manufacturer type A, B or C.

4. Results

4.1. Si

To assess the sensitivity of the PL mapping for defect detection a number of micro-scans were recorded and then these regions were laser marked before defect etching. The wafers were scanned with low resolution to obtain the fastest and most accurate way of detecting defects. Figure 2 shows the defects detected using PL micro-mapping from a Si wafer following a high-temperature thermal treatment (the individual defects are labelled). Figure 3 shows exactly the same location after defect etching and there is a clear one-to-one correlation. This trend is consistent at the other locations on the wafer and also on the other wafers. Figure 4 shows the spatial variation of the defect density detected by SiPHER and also shows how the defect density determined by defect etching follows the same trend. These results show that PL mapping using SiPHER can be used as a non-destructive alternative to defect etching.

4.1.1. Slip in 300 mm wafers. A whole-wafer PL map shows quite clearly edge slip on a thermally processed 300 mm Si wafer (figure 5). These slip lines can also be observed on the back of the wafer as well. The other wafers in this batch did not show edge slip. One set of 300 mm epi-wafers from another Si supplier was also inspected. All the wafers had slip marks at set positions (separated exactly by 120°) on the back of all the wafers but not on the front surface (figure 6). Clearly PL mapping can be applied to detect slip using whole-wafer

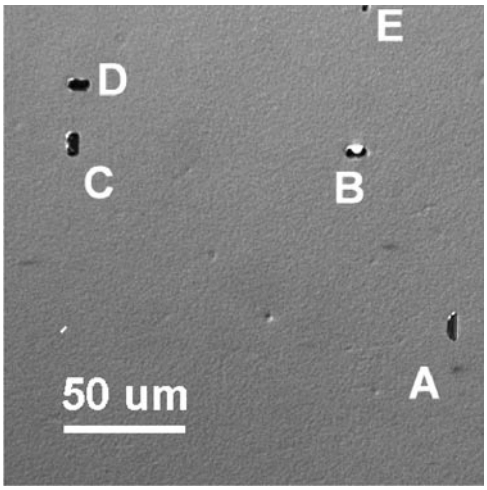

Figure 3. The same location as shown in figure 2 after defect etching.

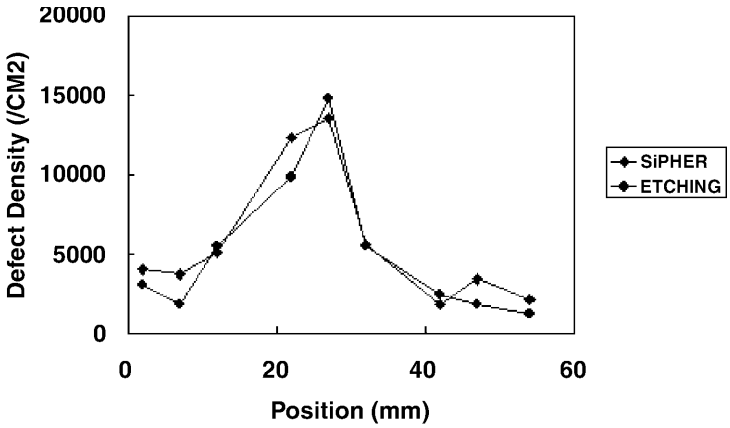

Figure 4. Defect density as determined by both PL mapping (SiPHER) and defect etching.

mapping. Also the micro-scanning capability facilitates the inspection of slip on the very edge of the wafer across the bevel edge.

4.2. SiGe epilayers

A selection of SiGe wafers with different thickness and composition were analysed. Whole-wafer maps were recorded and then the defective areas were re-scanned at higher resolution. The main defect types observed are discussed in detail in the next sections.

4.2.1. Manufacturer A, 150 mm SiGe 6% 130 nm. Most of the wafers in this wafer batch were very good quality, except one wafer which showed a distinct area of PL non-uniformity at the bottom of the wafer region covering approximately 2–3 cm^2 (6% Ge and thickness 130 nm). A micro-scan (see figure 7) was recorded in the area of reduced PL and revealed a low density ($\approx$100 cm^{-2}) of dark line defects lying in the two orthogonal $\langle 110 \rangle$ interfacial directions. These features are attributed to recombination at interfacial misfit dislocations. On

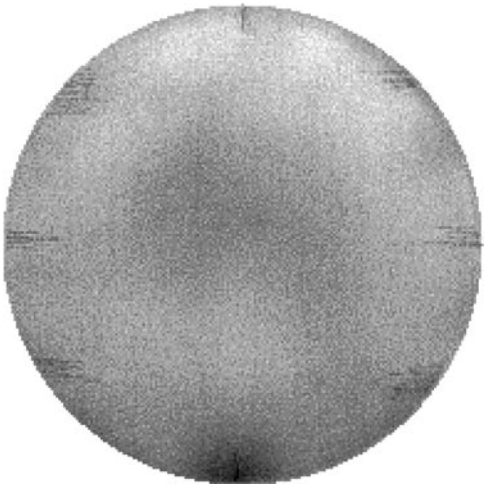

Figure 5. PL map of a 300 mm wafer revealing slip.

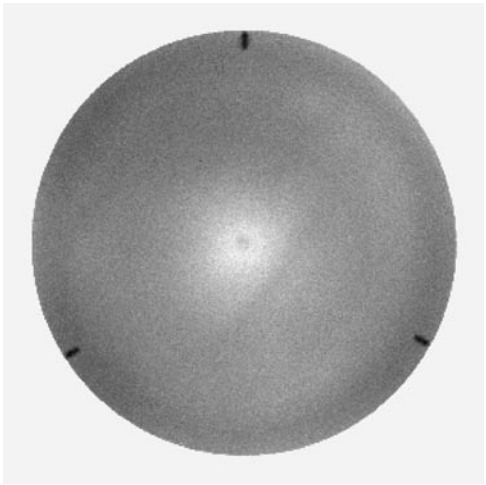

Figure 6. PL map of a 300 mm wafer revealing slip marks on the wafer back surface.

closer inspection of the defect images the misfit dislocations were observed to have enhanced recombination only at one end (see figure 8).

4.2.2. Manufacturer B, 200 mm SiGe 13% 280 nm. This wafer contained a high number of defects directly observed in the PL map. Closer inspection of these wafers revealed a nucleation point surrounded by a very high density of misfit dislocations. A typical example is shown in figure 9. On closer inspection and by varying the image contrast one can see that there is a nucleation centre visible in the PL image. Direct comparison with the surface map image reveals that the nucleation centre is actually a particle (figure 10).

4.2.3. Manufacturer C, 200 mm Si (750 Å)/SiGe (500 Å 25%). This type of wafer contained a moderate density defect $\approx$200 cm^{-2} observed in the PL map (figure 11). Following closer

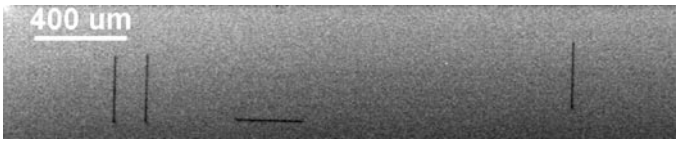

Figure 7. PL map revealing a low density of misfit dislocations.

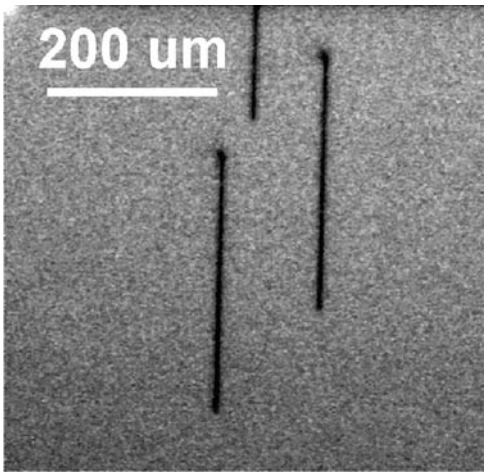

Figure 8. A high-resolution PL map revealing misfit dislocations in more detail.

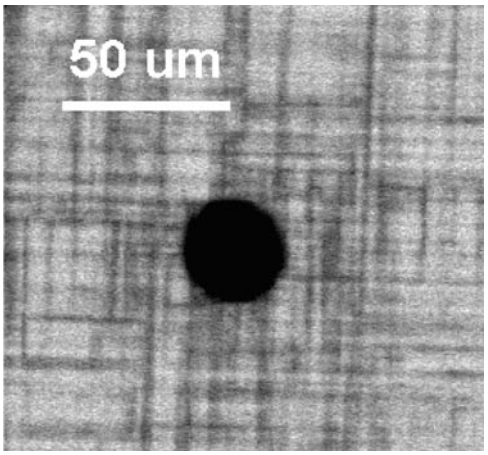

Figure 9. PL map showing a high density of misfit dislocations.

examination these defects had a very irregular shape. An example of this defect type is shown in figure 12. The defects could also be observed in optical DIC images (figure 13). This defective region and adjacent areas in this sample were further examined using atomic force microscopy (AFM) and plan view TEM. Figure 14 shows the AFM image of the defective region: it consists of a many broad shallow pits approximately 2–3 nm deep. The bottom of the pit is considerably rougher than the surrounding Ge_xSi_{1-x} surface (approximately 8 nm peak to pit). Figure 15 shows a plan view TEM image of a small defective region close to

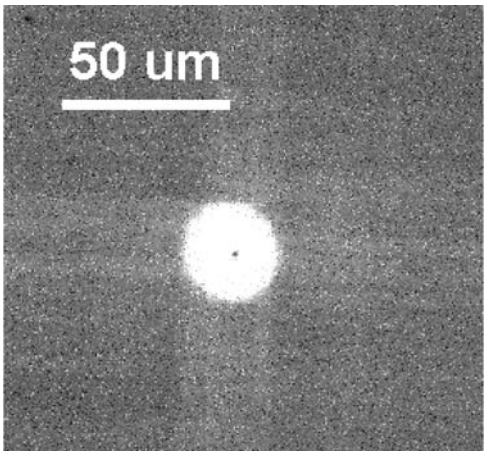

Figure 10. Surface reflection map of same location as shown in figure 9.

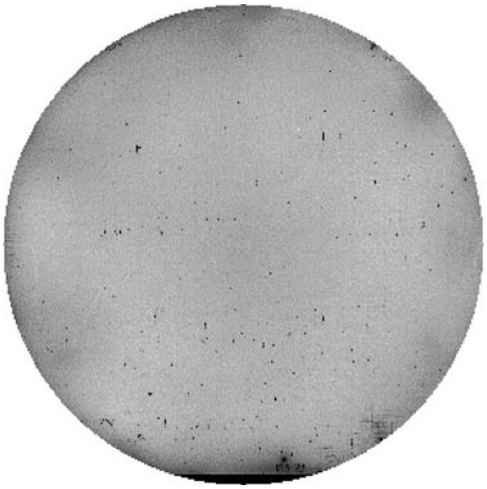

Figure 11. PL map of SiGe epilayer revealing defective regions.

those shown in figure 14. An array of misfit dislocations is present at the Ge_xSi_{1-x}/Si interface outside the defective region; inside the defective region a very high density of dislocation loops and stacking faults is present. Figure 16 shows the edge of the region in more detail. The high density of dislocations in the defective region act as sources for misfit dislocations which then propagate along the Ge_xSi_{1-x}/Si interface.

5. Discussion

PL mapping is an ideal non-destructive method for defect detection: a range of different defect types can be detected, and in some specific cases their structure can be revealed from the defect contrast in terms of geometry or shape [5]. The defects are observed due to their effect on the recombination lifetime; there is a significant amount of evidence that extrinsic factors such as impurity interactions and defect decoration control the recombination properties of defects [9, 19]. It therefore follows that defects are revealed due to their impurity decoration and the

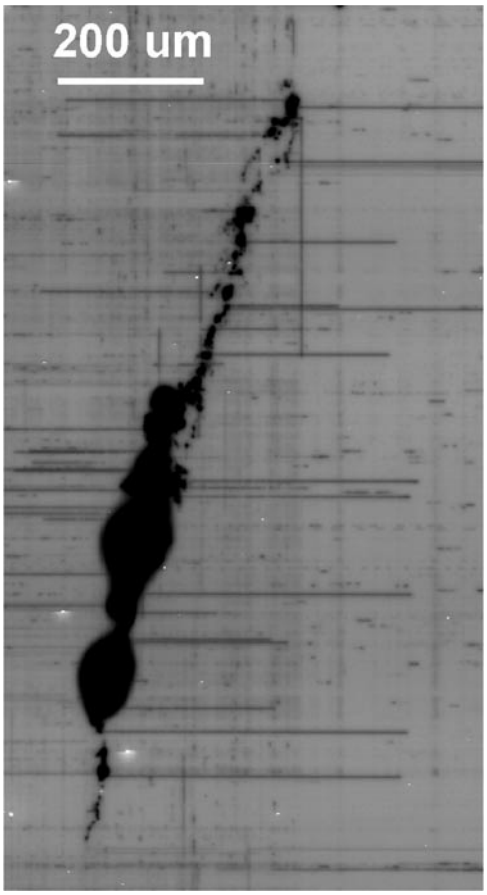

Figure 12. PL map revealing a large defective region.

true nature of the defect may not be apparent. However, because the defect co-ordinates are known, the defect location can be precisely located using laser marking to facilitate TEM analysis to fully identify the defect [21].

Another important application is the detection of slip on Si wafers and Si epilayers. Even today state-of-the-art IC companies can have device yield loss maps, due to thermal slip. These maps follow the thermal slip predicated by Hu [22] for conditions of both high and moderate stress levels. This problem is more critical for 300 mm wafers, because the yield stress at elevated temperatures is just a few MPa. Also because the gravity induced bending stress can be larger than 3 MPa, plastic deformation will occur if precautions are not taken (e.g. design of vertical wafer boats for thermal treatments) [23]. Slip can occur prior to (during pre-gettering treatments and during diffusion or implantation) or during epitaxial growth. Slip can also be produced after epitaxial growth if the thermal/cooling cycles are too extreme.

The 300 mm PL wafer map we have shown in figure 4 shows the slip distribution relating to a high thermal stress as predicted by Hu [22]. Using a different support holder eliminated this particular slip issue. The PL map of the 300 mm epilayer wafer, in figure 5 reveals slip marks detected on the back of the wafer: this is due to design and location of the lift pins in the epitaxial reactor producing large thermal stresses. This problem was rectified by redesign of the lift mechanism.

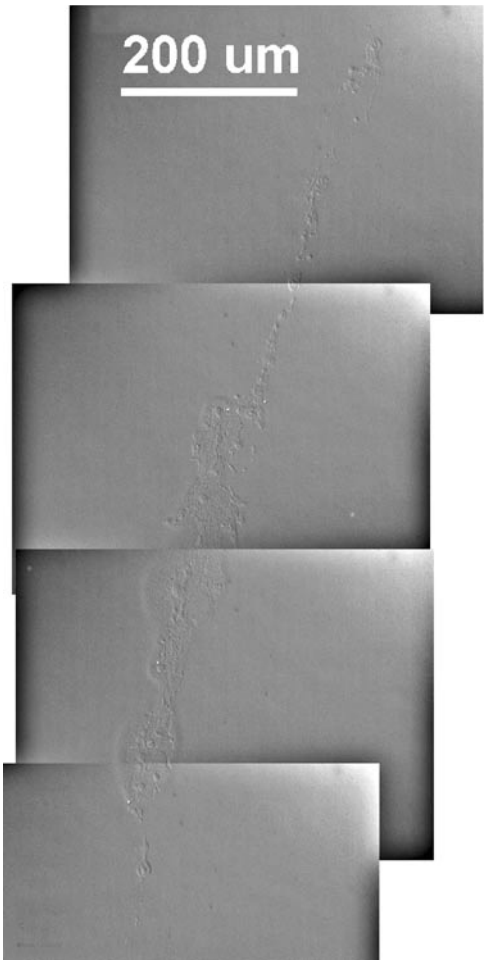

Figure 13. Nomarski optical image of the defective area in figure 12.

The PL mapping method detects slip due to the electrical activity of the slip dislocations and defect produced during thermal slip. This raises the question of whether all slip lines are electrically active. In all the wafers we have analysed to date we have found a good correlation of PL mapping with other methods. Also although the contamination levels in state of the art processing are very low, slip formation will act as a perfect nucleation site for any residual impurities, which can be gettered, and these impurities produce electrical activity. Also we have already shown that this technique is extremely sensitive and can detect defects whose recombination properties are controlled by shallow levels, which cannot be detected by EBIC at room temperature [21]. Further experiments are under way to clarify the activity of slip defects using combined TEM/EBIC and PL mapping.

The relaxation of strained layers, both III–V layers and Ge_xSi_{1-x} layers such as those described in section 4.2, has been found to occur in several stages (e.g. Beanland *et al* [24] and Fitzgerald [25]). First, in layers below the critical thickness h_c, existing defects such as threading dislocations are replicated in the epitaxial layer, but their self-stress is higher than the force they experience due to the misfit stress, and so they remain immobile. Second, as

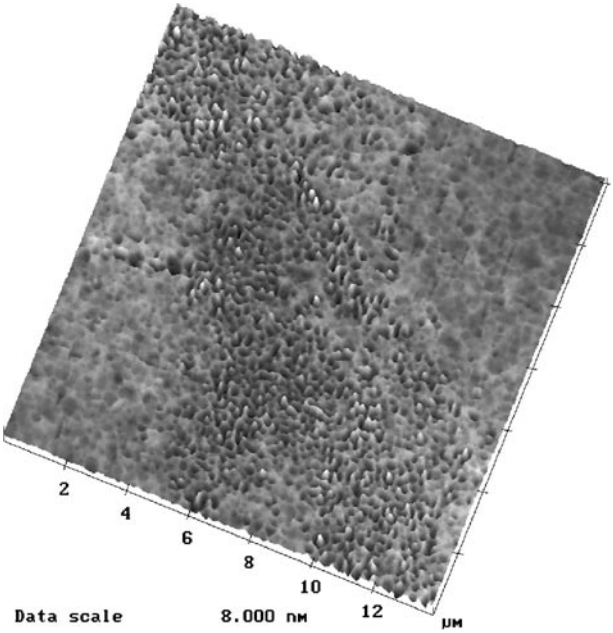

Figure 14. AFM image of part of the defective region in figure 12.

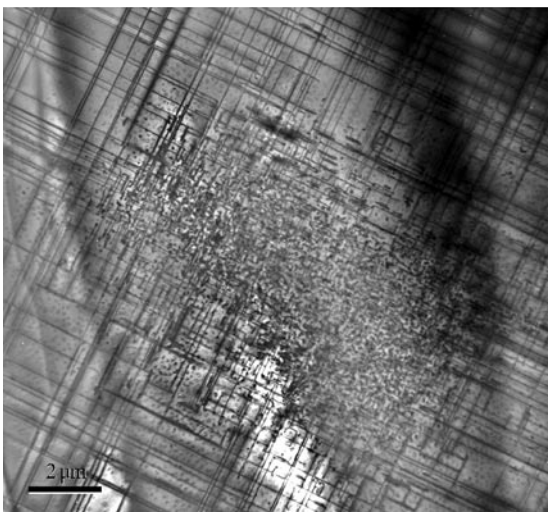

Figure 15. Bright-field TEM image of a small defective region. A very high density of dislocations can be seen at the defect site.

the critical thickness is passed, these defects begin to move and form misfit dislocations in the interface, with a threading segment running from one end of the misfit dislocation to the epilayer surface [26]. The mobility of the threading dislocations increases with the 'excess stress' [27]—i.e. the difference between the misfit stress and the self-stress of the threading dislocation—and temperature. Third, when the layer reaches about four times the critical thickness, dislocation multiplication can occur [28] and the dislocation density can

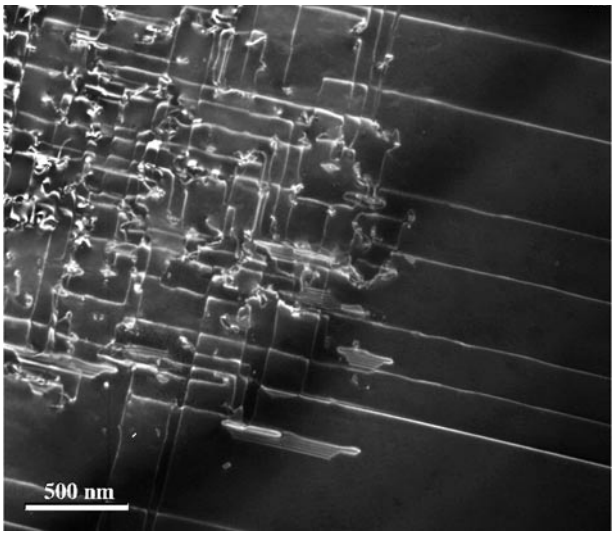

Figure 16. Dark-field, weak-beam ($\boldsymbol{g}$, $2\boldsymbol{g}$ 220) image of the edge of a defective region.

increase significantly. Finally, as the threading dislocation density increases and the strain drops, work-hardening effects begin to dominate and the rate of relaxation slows once more. The microstructure observed in an epitaxial layer can thus take on a variety of forms dependent upon the growth rate, initial dislocation source density temperature and layer thickness. If any of these parameters vary across a wafer, variations in microstructure would be expected to occur.

Our observations show that the whole-wafer maps have shown local areas of reduced PL intensity. This may be associated with inhomogeneities in layer composition or thickness, which are in turn due to the effects of contamination prior to or during growth. These effects can thus cause relaxation to occur on a local scale. Furthermore, such effects can provide dislocation sources, which will propagate into the surrounding material if the dislocation mobility is sufficiently high. It is thus not surprising to observe high concentrations of defects that may extend some distance from contamination sites.

The low density of misfit dislocations observed in wafer from manufacturer A (figures 7 and 8) has a unique character. This defect structure is consistent with the earliest stages of relaxation in a layer, which has just passed the critical thickness h_c. Each short segment of misfit dislocation has been produced by the extension of a dislocation threading through the layer from the substrate. These threading dislocations begin to move once the critical thickness is exceeded, and continue to do so until the temperature drops sufficiently to reduce their mobility (essentially zero at room temperature). The identical length of each misfit dislocation indicates that all the threading dislocations began to move at the same time, and all have the same mobility. The microstructure would be expected to be thermally unstable, with further relaxation occurring if the temperature is increased sufficiently to allow the dislocation mobility to become significant once more. Note also the different appearance of each end of the misfit dislocation. On each dislocation there is a curved end exhibiting enhanced recombination (probably corresponding to the threading segment) and a straight end (probably corresponding to the segment in the bulk of the material).

Another commonly observed defect type is a nucleation source surrounded by a very high density of misfit dislocations (figures 9 and 10). The small circular defects are almost certainly

particle related. It may be expected that relaxation—due to nucleation of misfit dislocations at particles—would show a dependence upon the particle size. Larger particles would be expected to induce higher stresses (e.g. due to thermal mismatch effects or chemical reactions with the layer). As this stress would generally add to the misfit stress, the initial relaxation of layers with higher Ge compositions will be more sensitive to particulate contamination. However, once the misfit dislocation density is sufficiently high to be limited by work-hardening effects and dislocation multiplication (as in this sample), particulate density will have only a limited impact on misfit dislocation density.

The irregularly shaped defects, which both give strong recombination observed by SiPHER (figure 12) and exhibit surface roughness which can be detected by DIC optical microscopy (figures 13) and AFM (figure 14), probably form due to metallic contamination of the wafer prior to growth. This is consistent both with the high recombination at the defect site and the high density of defect loops and stacking faults observed by plan view TEM (figure 16). There is also discontinuous contrast visible in figure 11 that clearly originates from the misfit dislocation array rather than the primary contamination site. It may be those dislocations with particular Burgers vectors (e.g. 90° $\frac{1}{2}$[110] rather than 60° $\frac{1}{2}\langle 101\rangle$) act as stronger recombination sites in this sample. The high density of defects in the contaminated regions has a strong effect on the growth rate of the epitaxial layer, producing surface roughness in the same manner as the cross-hatch pattern observed on the surface of layers with significant densities of misfit dislocations [29].

6. Conclusions

Several Ge_xSi_{1-x}/Si structures have been examined using SiPHER. Some of the defects observed were also examined using a variety of other techniques, i.e. optical differential interference microscopy, scanning probe microscopy and plan view TEM. The ability to examine whole wafers in SiPHER allows rapid identification of inhomogeneities and defects, which can be understood in terms of models of the relaxation of strained epitaxial layers and the effect of metallic contamination on dislocation formation.

Acknowledgments

The authors would like to thank Martin Kittler (Institut für Halbleiterphysik) and Bob Jones (University of Exeter) for stimulating discussions about PL and EBIC measurements.

References

[1] Drozdov N A, Patrin A A and Tkachev V D 1976 *Sov. Phys.–JETP Lett.* **23** 597
[2] Sauer R, Weber J, Stolz J, Weber E R, Küsters K H and Alexander H 1985 *Appl. Phys.* A **36** 1
[3] Higgs V, Lightowlers E C, Norman C E and Kightley P 1992 *Mater. Sci. Forum* **83** 1309
[4] Higgs V and Kittler M 1993 *Appl. Phys. Lett.* **63** 2085
[5] Higgs V, Chin F, Wang X, Kitagawara Y and Yoshida Y 1998 *Semiconductor Silicon* ECS PV 98-1, ed H R Huff *et al* (Pennington, NJ: Electrochemical Society) p 1564
[6] Suezawa M, Sasaki Y, Nishina Y and Sumino K 1981 *Japan. J. Appl. Phys.* **20** L537 183
[7] Weronek K, Weber J, Hopner A, Ernst F, Buchner R, Stefaniak M and Alexander H 1992 *Mater. Sci. Forum* **83** 1315
[8] Lelikov Yu S, Rebane Yu T and Shreter Yu G 1989 *Structures and Properties (Inst. Phys. Conf. Ser. 104)* (Bristol: Institute of Physics) p 119
[9] Kittler M, Kveder V V and Schroter W 1999 *Solid State Phenom.* **69** 417
[10] Suezawa M and Sumino K 1983 *Phys. Status Solidi* **78** 639
[11] Osipyan Y A, Rtishchev A M, Steinman E A, Yakimov E B and Yarykin N A 1982 *Sov. Phys.–JETP* **55** 294

[12] Pizzini S, Binetti S, Acciarri M and Casati M 2000 *Mater. Res. Soc. Symp. Proc.* vol 588 (Pittsburgh, PA: Materials Research Society) p 117
[13] Weber J and Alonso M I 1989 *Defect Control in Semiconductors* ed K Sumino Yokohama (Amsterdam: Elsevier–North-Holland)
[14] Higgs V, Goulding M, Brinklow A and Kightley P 1992 *Appl. Phys. Lett.* **60** 1369
[15] Higgs V, Zhou T Q and Rozgoni G A 1994 *Mater. Sci. Eng.* B **24** 48
[16] Higgs V 1996 *Early Stages of Oxygen Precipitation in Silicon (NATO ASI 3. High Technology 17)* ed R Jones (Dordrecht: Kluwer) p 469
[17] Higgs V, Lightowlers E C, Tajbakhsh S and Wright P J 1992 *Appl. Phys. Lett.* **61** 1087
[18] Tajima M, Tokita M and Warashina M 1995 *Mater. Sci. Forum* **196** 1749
[19] Kittler M, Bouillet-Ulhaq C and Higgs V 1995 *J. Appl. Phys.* **78** 4573
[20] Hayamizu Y, Hoshi R, Kitagawara Y and Takenaka T 1995 *Proc. SPIE* **2638** 113
[21] Higgs V, Chin F and Wang X 1998 *Solid State Phenom.* **63** 421
[22] Hu S M 1977 *J. Vac. Sci. Technol.* **14** 17
[23] Xin P 1998 *Semiconductor Silicon* ECS PV 98-1, ed H R Huff *et al* (Pennington, NJ: Electrochemical Society) p 660
[24] Beanland R, Dunstan D J and Goodhew P J 1996 *Adv. Phys.* **45** 87
[25] Fitzgerald E A 1991 *Mater. Sci. Rep.* **7** 91
[26] Matthews J W and Blakeslee A D 1974 *J. Cryst. Growth* **27** 118
[27] Dodson B W and Tsao J Y 1988 *Appl. Phys. Lett.* **51** 1325
[28] Beanland R J 1992 *Appl. Phys.* **72** 4031
[29] Shiryaev Yu S, Jensen F and Petersen J W 1994 *Appl. Phys. Lett.* **64** 3305